Inorganic Chemistry

Article

pubs.acs.org/IC

Azadipyrromethene Dye Derivatives in Coordination Chemistry: the Structure–Property Relationship in Homoleptic Metal(II) Complexes

André Bessette,[†,‡] Janaina G. Ferreira,[†] Martin Giguère,[‡] Francis Bélanger,[‡] Denis Désilets,[‡] and Garry S. Hanan*,[†]

[†]Département de Chimie, Université de Montréal, Pavillon J.-A. Bombardier, 5155 Decelles Avenue, Montréal, Québec H3T-2B1, Canada

[‡]Saint-Jean Photochimie Inc., 725 Trotter Street, Saint-Jean-sur-Richelieu, Québec J3B 8J8, Canada

Supporting Information

ABSTRACT: As a chromophore closely related to dipyrromethene (DPM), the azadipyrromethene (ADPM) family has attracted much interest in the life sciences and optoelectronic fields. A high-yielding microwave-assisted synthesis is reported for new homoleptic complexes of cobalt(II), nickel(II), copper(II) and zinc(II) based on the tetrakis(*p*-methoxyphenyl)-azadipyrromethene ligand **1b**. These complexes are compared with other homoleptic complexes of the same metal(II) series based on the tetraphenylazadipyrromethene **1a** and also with related BF_2^+ chelates (Aza-BODIPYs **6a** and **6b**) for a better understanding of trends arising from substitution of the chelate and/or the electron-donating effect of the *p*-methoxy substituents. The electrochemical behavior of the new compounds **2b**, **3b**, and **5b** in dichloromethane revealed two pseudoreversible reductions (**2b**, −1.09 and −1.25 V vs SCE; **3b**, −1.05 and −1.29 V; **5b**, −1.13 and −1.25 V) followed by a third irreversible process (**2b**, −1.78 V; **3b**, −1.80 V; **5b**, −1.77 V) along with two pseudoreversible oxidations (**2b**, 0.55 and 0.80 V; **3b**, 0.56 and 0.80 V; **5b**, 0.55 and 0.80 V) followed by two closely spaced irreversible processes (**2b**, 1.21 and 1.27 V; **3b**, 1.21 and 1.28 V; **5b**, 1.22 and 1.25 V). On its side, copper(II) homoleptic complex **4b** revealed only one pseudoreversible reduction at −0.59 V followed by three irreversible processes at −0.95, −1.54, and −1.74 V, respectively. The oxidation behavior of this complex exhibited two pseudoreversible processes (0.55 and 0.82 V) and two irreversible processes (1.19 and 1.25 V). The redox processes are assigned and discussed in relation to their photophysical properties. X-ray structures for **1b** and related copper(II) complex **2b** are also discussed.

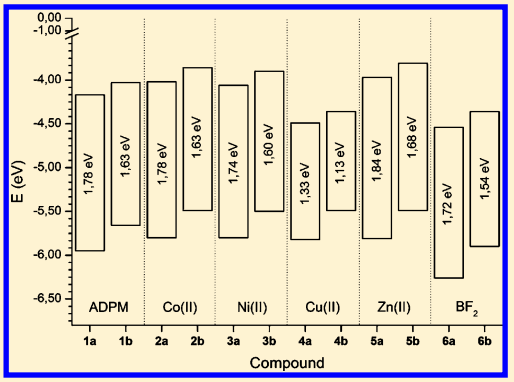

INTRODUCTION

Dipyrromethene (DPM) organic dyes have attracted attention because of their practical applications, e.g., biological probes[1] and light-harvesting[2] system components. As a close relative of this intense red-absorbing and near-infrared (NIR)-emitting compound, azadipyrromethene (ADPM) offers an opportunity to absorb and emit even further in the red and NIR regions, respectively. Therefore, this family of chromophores is attracting increased interest, especially in organometallic chemistry.[3] In fact, ADPM exhibits properties similar to those of the DPM family including versatile methods of preparation,[4] even for unsymmetrical derivatives.[5] Consequently, fine-tuning of the optical and steric properties becomes feasible for the preparation of suitable photoactive materials for life sciences and solar energy conversion, including photovoltaic applications.[6] Unlike DPM, the ADPM dye has never been isolated in its unsubstituted form, being mainly formed as tetraaryl derivatives in the 3 and 5 positions by two distinct synthetic methods.[4] Figure 1 depicts both generic chromophores and their classical boron adducts (BODIPY and Aza-BODIPY) with the position numbering and corresponding nomenclature.

The synthesis of homoleptic complexes of the d^{10} metal ions zinc(II) and mercury(II) with various substituted tetraarylazadipyrromethenes was recently reported by Gray and coworkers.[7] Subsequently, O'Shea et al. studied the spectroscopic properties of cobalt(II), nickel(II), copper(II), and zinc(II) chelates **2a**–**5a** based on tetraphenylazadipyrromethene **1a** (Figure 2),[8] 66 years after their initial synthesis by Rogers.[9]

The synthesis of ADPM-based homoleptic complexes was ameliorated by O'Shea et al. as the reaction time was decreased from 1 day at room temperature (rt) in tetrahydrofuran (THF) to about 1 h in hot *n*-butanol, although this procedure was not high-yielding in every case. Herein, we report a new synthetic approach using microwave-assisted heating and potassium *tert*-butoxide (KO^tBu) as a strong base to deprotonate the pyrrolic unit. This optimization of conditions led to a more straightforward, high-yielding, and reproducible synthesis on the time scale of minutes. This procedure allowed us to prepare new homoleptic four-coordinate complexes of cobalt(II), nickel(II), copper(II), and zinc(II), **2b**–**5b**, featuring the

Received: April 28, 2012

   dx.doi.org/10.1021/ic300872m | *Inorg. Chem.* XXXX, XXX, XXX–XXX

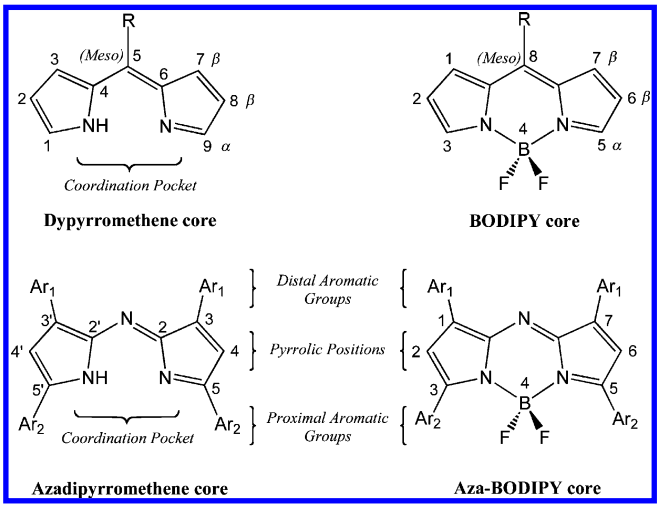

Figure 1. DPM, ADPM, and their corresponding boron adducts.

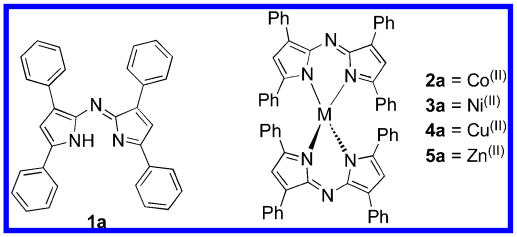

Figure 2. ADPM ligand **1a** and complexes **2a**–**5a**.

tetrakis(*p*-methoxyphenyl)-substituted ADPM ligand **1b** also reported by Rogers[9] and absent from the scientific literature since then (Scheme 1).

In addition to characterization by ^{1}H and ^{13}C NMR, high-resolution mass spectrometry (HRMS), and elemental analysis, electrochemistry has been used to establish the exact energy associated with the highest occupied molecular orbital (HOMO) and lowest unoccupied molecular orbital (LUMO) levels of ligands **1a** and **1b**, complexes **2**–**5b**, and Aza-BODIPYs **6a** and **6b** (Figure 3). Because of an emergent area of ADPM coordination chemistry, the effect of metal complexation and also of substitution with electron-rich methoxy groups on the electronic properties of this dye family was still be lacking from an electrochemical point of view. In order to establish a general trend, the photophysical characterization of those new electron-rich tetra-*p*-methoxy compounds is also reported and compared to existing tetraphenylazadipyrromethene derivatives in both dichloromethane (DCM, $CDCl_3$) and THF solution. Finally, X-ray structures of **1b** and **2b** are discussed in relation to existing results observed for similar homoleptic metal(II) complexes in order to have insight on the effect of the electron-rich tetrakis(*p*-methoxyphenyl)-azadipyrromethene. All together, information presented herein should permit an empirical evaluation of such chromophores toward their incorporation in photovoltaic applications as electron-donor or photosensitizer materials.[1f,6k,l,10]

EXPERIMENTAL SECTION

1. Materials and Instrumentation. Literature procedures were used for the synthesis of compounds **1a**, **1b**, **2**–**5a**, and **6a**.[4,8] Aza-BODIPY **6b** was obtained from Saint-Jean Photochemicals Inc. and used as received. $M(OAc)_2{\cdot}xH_2O$ (M = Co, Ni, Cu, Zn; OAc = acetate), potassium *tert*-butoxide (KO^tBu), and solvents were obtained commercially and used without further purification. Reactions were

Scheme 1. Synthesis of Complexes 2b–5b from ADPM Ligand 1b Assisted by Microwave Irradiation

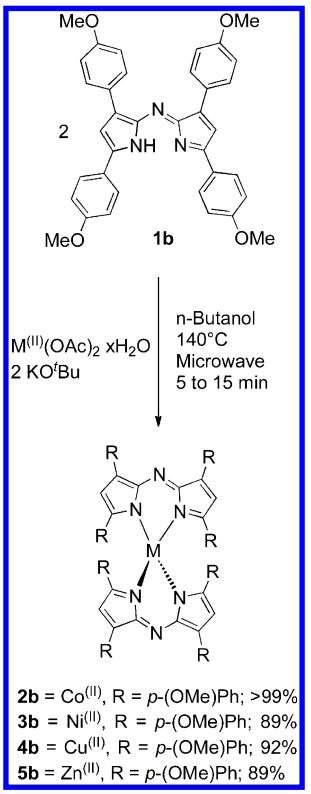

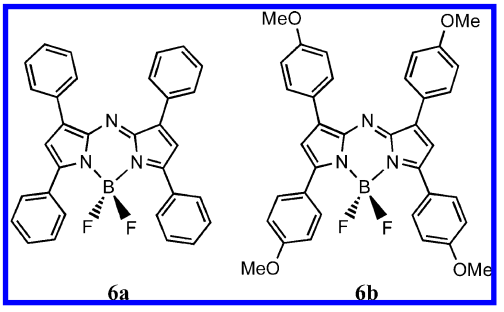

Figure 3. Aza-BODIPYs **6a** and **6b**.

carried out under an ambient atmosphere. Solvents were removed under reduced pressure using a rotary evaporator unless otherwise stated.

Microwave reactions were performed on a Biotage Initiator 8 equipped with an autosampler in 20 mL flasks from the same distributor. The degree of absorption was set to normal, with 2 min of prestirring and a stirring rate of 600 rpm.

Nuclear magnetic resonance (NMR) spectra were recorded in $CDCl_3$ at rt on a Bruker AV400 spectrometer at 400 MHz for ^{1}H NMR and at 100 MHz for ^{13}C NMR, otherwise stated. Chemical shifts are reported in part per million (ppm) relative to residual solvent protons (7.26 ppm for chloroform-*d*) and the carbon resonance of the solvent (77.16 ppm for chloroform-*d*). Absorption and emission spectra were measured in CH_2Cl_2 and THF at concentrations obeying Beer–Lambert's law at rt on a Cary 500i UV–vis–NIR spectrophotometer and a Cary Eclipse fluorescence spectrophotometer, respectively.

High-resolution electrospray ionization mass spectrometry (HR-ESIMS) was performed by liquid chromatography/mass spectrometry with a time-of-flight detector (LC/MS TOF) from Agilent by infusion of a solution in CH_2Cl_2 of compounds **2**–**5b** directly into the source by vacuum aspiration.

dx.doi.org/10.1021/ic300872m | *Inorg. Chem.* XXXX, XXX, XXX–XXX

Electrochemical measurements were carried out in argon-purged CH_2Cl_2 at rt with a BAS CV50W multipurpose equipment interfaced to a PC. The working electrode used was a glassy carbon electrode for every compound. The counter electrode was a platinum wire, and the pseudoreference electrode was a silver wire. The reference was set using an internal 1 mM ferrocene/ferrocenium sample at 0.46 V vs SCE in CH_2Cl_2. The concentration of the compounds was about 1 mM. Tetrabutylammonium hexafluorophosphate (TBAP) was used as the supporting electrolyte, and its concentration was 0.10 M. Cyclic voltammetry (CV) scans were obtained at scan rates of 50, 100, 200, and 500 mV/s. For reversible processes, half-wave potentials (vs SCE) from CV were used. To establish the potential of irreversible processes, differential pulse voltammetry (DPV) experiments were performed with a step rate of 4 mV, a pulse height of 50 mV, and a frequency of 5 Hz. Criteria for reversibility were the separation of 60 mV between the cathodic and anodic peaks, the close-to-unity ratio of the intensities of the cathodic and anodic currents, and the constancy of the peak potential with changing scan rate.

Diffraction data were collected on a Bruker Microstar diffractometer equipped with a Platinum 135 CCD detector, a Helios optics, a Kappa goniometer, and Cu Kα radiation. The diffraction quality of the crystals were checked several times, revealing in all cases poor diffraction with a large amount of diffuse scattering, signaling extensive crystal disorder. Cell refinement and data reduction were done using *APEX2*.[11] Absorption corrections were applied using *SADABS*.[12] Structures were solved by direct methods using *SHELXS97* and refined on F^2 by full-matrix least squares using *SHELXL97*.[13] All non-hydrogen atoms were refined anisotropically. Hydrogen atoms were refined isotropically on calculated positions using a riding model. For compound **1b**, the highest residual difference peak with an electronic density of 1.4 e/Å^3 is essentially due to a minor spatial disorder of the N2 atom (evaluated to 18%) and was not modeled in the final structure. For the nickel(II), cobalt(II), and copper(II) complexes, crystals showed high mosaicity and low diffraction, as well as high decay of standard intensities during data collection (around 20%). Because of the undesirable characteristics described above, the crystal structures of the nickel, copper, and zinc complexes were not completed. However, it was possible to determine details of the connectivity and conformation from those complexes, which were similar to those obtained for the distorted tetrahedral cobalt complex **2b**. For this last complex, the structure exhibited high disorder, mainly over the methoxyphenyl rings, which was modeled as two components, with an average ratio of 0.7/0.3, and refined anisotropically.

Experimental uncertainties are as follows: absorption maxima, ±2 nm; molar absorption coefficient, 10%; emission maxima, ±5 nm; redox potentials, ±10 mV.

2. Experimental Procedures and Data. *Bis[3,5-bis(4-methoxyphenyl)-1H-pyrrol-2-yl-3,5-bis(4-methoxyphenyl)-2-ylideneamine]-cobalt(II) (**2b**).* A suspension of compound **1b** (116 mg, 0.203 mmol), cobalt(II) acetate tetrahydrate [$Co(OAc)_2{\cdot}4H_2O$; 25 mg, 0.10 mmol], and KO^{t}Bu 95% (24 mg, 0.20 mmol) in *n*-butanol (10 mL) was reacted in a microwave reactor for 15 min under magnetic stirring. The reaction mixture was evaporated to dryness, dissolved in CH_2Cl_2, and filtered through Celite. The solvent was evaporated to afford a blue-purple powder. Yield: 123 mg (>99%). ^{1}H NMR ($CDCl_3$, 500 MHz): δ 7.22 (br s), 7.84 (br s), 8.73 (br s), 15.02 (br s), 15.33 (br s), 63.66 (br s). HR-ESIMS. Calcd for $C_{72}H_{60}N_6O_8Co$ ([M$^+$]): m/z 1195.3799. Found: m/z 1195.3781. Elem anal. Calcd: C, 72.29; H, 5.06; N, 7.03. Found: C, 72.23; H, 5.07; N, 7.00. Crystals suitable for X-ray analysis were obtained from double-layer crystallization in CH_2Cl_2 and hexanes.

*Bis[3,5-bis(4-methoxyphenyl)-1H-pyrrol-2-yl-3,5-bis(4-methoxyphenyl)-2-ylideneamine]nickel(II) (**3b**).* A suspension of compound **1b** (117 mg, 0.206 mmol), nickel(II) acetate tetrahydrate [$Ni(OAc)_2{\cdot}4H_2O$; 26 mg, 0.10 mmol], and KO^{t}Bu 95% (24 mg, 0.20 mmol) in *n*-butanol (10 mL) was reacted in a microwave reactor for 10 min under magnetic stirring. The reaction mixture was evaporated to dryness, dissolved in CH_2Cl_2, and filtered through Celite. The solvent was evaporated, and the resulting red-purple residue was concentrated in THF and recrystallized by the slow diffusion of pentane. The solid was isolated by filtration and washed with pentane (3 × 5 mL), which afforded a red-purple powder. Yield: 109 mg (89%). ^{1}H NMR ($CDCl_3$, 400 MHz): δ −1.78 (d, J = 7.46 Hz, 8 H), 2.79 (s, 12 H), 3.44 (s, 12 H), 6.40 (d, J = 7.67 Hz, 8 H), 8.15 (br s, 8 H), 34.53 (br s, 8 H), 61.52 (br s, 4 H). HR-ESIMS. Calcd for $C_{72}H_{60}N_6O_8Ni$ ([M$^+$]): m/z 1194.3821. Found: m/z 1194.3828. Elem anal. Calcd: C, 72.31; H, 5.06; N, 7.03. Found: C, 72.30; H, 4.97; N, 7.08.

*Bis[3,5-bis(4-methoxyphenyl)-1H-pyrrol-2-yl-3,5-bis(4-methoxyphenyl)-2-ylideneamine]copper(II) (**4b**).* A suspension of compound **1b** (118 mg, 0.207 mmol), copper(II) acetate monohydrate [$Cu(OAc)_2{\cdot}H_2O$; 21 mg, 0.10 mmol], and KO^{t}Bu 95% (25 mg, 0.21 mmol) in *n*-butanol (10 mL) was reacted in a microwave reactor for 5 min under magnetic stirring. The reaction mixture was evaporated to dryness, dissolved in CH_2Cl_2, and filtered through Celite. The solvent was evaporated, and the resulting blue-purple residue was concentrated in THF and recrystallized by the slow diffusion of pentane. The solid was isolated by filtration and washed with pentane (3 × 5 mL), which afforded a blue-purple powder. Yield: 114 mg (92%). HR-ESIMS. Calcd for $C_{72}H_{60}N_6O_8Cu$ ([M$^+$]): m/z 1199.3763. Found: m/z 1199.3734. Elem anal. Calcd: C, 72.01; H, 5.04; N, 7.00. Found: C, 71.79; H, 5.23; N, 6.83.

*Bis[3,5-bis(4-methoxyphenyl)-1H-pyrrol-2-yl-3,5-bis(4-methoxyphenyl)-2-ylideneamine]zinc(II) (**5b**).* A suspension of compound **1b** (142 mg, 0.249 mmol), zinc(II) acetate dihydrate [$Zn(OAc)_2{\cdot}2H_2O$; 27 mg, 0.13 mmol], and 95% KO^{t}Bu (29 mg, 0.25 mmol) in *n*-butanol (10 mL) was reacted in a microwave reactor for 5 min under magnetic stirring. The reaction mixture was evaporated to dryness, dissolved in CH_2Cl_2, and filtered through Celite. The solvent was evaporated, and the resulting red-purple residue was concentrated in THF and recrystallized by the slow diffusion of pentane. The solid was isolated by filtration and washed with pentane (3 × 5 mL), which afforded a blue-purple powder. Yield: 134 mg (89%). ^{1}H NMR ($CDCl_3$, 400 MHz): δ 3.40 (s, 12 H), 3.92 (s, 12 H), 6.57−6.66 (m, 12 H), 6.97 (d, J = 8.78 Hz, 8 H), 7.44 (d, J = 8.78 Hz, 8 H), 7.89 (d, J = 8.78 Hz, 8 H). ^{13}C NMR ($CDCl_3$, 100 MHz): δ 55.01, 55.36, 72.21, 113.41, 113.42, 115.28, 126.05, 127.50, 128.31, 130.87, 143.93, 147.74, 159.28, 159.50, 160.45. HR-ESIMS. Calcd for $C_{72}H_{60}N_6O_8Zn$ ([M$^+$]): m/z 1200.3759. Found: m/z 1200.3724. Elem anal. Calcd: C, 71.90; H, 5.03; N, 6.99. Found: C, 71.73; H, 5.22; N, 6.76.

RESULTS AND DISCUSSION

Synthesis. Complexes **2a**−**5a** were obtained following literature procedures using ligand **1a**.[8] The new methodology developed to access complexes **2b**−**5b** consist of irradiating 2 equiv of **1b** with 1 equiv of the corresponding $M(OAc)_2{\cdot}xH_2O$ (M = Co, Ni, Cu, Zn; OAc = acetate) in the presence of 2 equiv of KO^{t}Bu at 140 °C in a microwave reactor for 5−15 min, using *n*-butanol as the solvent. Microwave irradiation accelerated the reaction while giving yields ranging from 89% to quantitative. The solvent, *n*-butanol, is suitable for such complexation because of its high boiling point, its stability toward side reactions and decomposition, and the ease of purification resulting from the insolubility of the product upon formation. Recrystallization was performed for each complex by the slow diffusion of pentane in a saturated solution of THF to remove residual traces of ligand, after filtration of salts on Celite in CH_2Cl_2. Dark-purple powders with tints of blue to red were isolated. Elemental analysis, ^{1}H and ^{13}C NMR [except for the paramagnetic copper(II) complex **4b**], and HRMS all supported conversion to the corresponding homoleptic complexes. The use of an aprotic solvent for MS gives the M$^+$ cation, while a proton source such as formic acid gives mainly the MH$^+$ species. Single crystals of the ligand **1b** and cobalt(II) complex **2b** suitable for X-ray diffraction were obtained from a double layer of DCM and hexanes.

dx.doi.org/10.1021/ic300872m | Inorg. Chem. XXXX, XXX, XXX−XXX

Table 1. Electrochemical Data for ADPM Ligands 1a and 1b, Complexes 2−5b, and Aza-BODIPYs 6a and 6b

compound	chelate			$E_{1/2}$(Ox)[a]			$E_{1/2}$(Red)[a]	
1a	none			1.36 (137)	1.01 (91)	−0.78 (72)	−1.45 (16)	
1b	none		1.30[b,c]	1.10[b,c]	0.71 (61)	−0.92 (106)	−1.52 (193)	
2a	Co^{II}			1.15 (102)	0.85 (97)	−0.93 (108)	−1.10 (104)	
2b	Co^{II}	1.27[b,c]	1.21[b,c]	0.80 (136)	0.55 (115)	−1.09 (109)	−1.25 (114)	−1.78[b,c]
3a	Ni^{II}			1.15 (111)	0.85 (106)	−0.89 (115)	−1.15 (113)	
3b	Ni^{II}	1.28[b,c]	1.21[b,c]	0.80[c] (111)[d]	0.56 (77)	−1.05 (86)	−1.29 (91)	−1.80[b,c]
4a	Cu^{II}			1.18 (95)	0.87 (86)	−0.46 (150)	−0.80 (88)	−1.41 (112)[e]
4b	Cu^{II}	1.25[b,c]	1.19[b,c]	0.82 (107)	0.55 (82)	−0.59 (106)	−0.95[c]	−1.54[f]
5a	Zn^{II}			1.15 (104)	0.86 (98)	−0.97 (111)	−1.11 (114)	
5b	Zn^{II}	1.25[b,c]	1.22[b,c]	0.80 (98)	0.55 (86)	−1.13 (82)	−1.25 (88)	−1.77[b,c]
6a	BF_2^+			1.45[c] (62)[d]	1.32 (122)	−0.40 (101)	−1.19 (96)	
6b	BF_2^+		1.52[b,c]	1.34[b,c]	0.95[b,c]	−0.58 (107)	−1.37 (92)	

[a]Potentials are in volts vs SCE for CH_2Cl_2 deaerated solutions, 0.1 M TBAP, recorded at 25 ± 1 °C at a sweep rate of 50 mV/s. The differences between the cathodic and anodic peak potentials (mV) are given in parentheses. [b]Irreversible. [c]Determined by DPV. [d]Obtained from CV before the addition of ferrocene. [e]Another pseudoreversible reduction process was observed at −1.60 (133) V (see the SI). [f]An irreversible reduction at −1.74 V was also observed by DPV (see the SI).

Electrochemistry. In the perspective of incorporating ADPM complexes in various photoactive systems, access to information concerning the energy levels of HOMO and LUMO becomes crucial in order to further fine-tune their properties. For instance, we can easily consider that a too low-lying LUMO level would not permit efficient electron transfer in potential photosensitizers for dye-sensitized solar cells or organic photovoltaic devices.[2c,14] Similarly, the photophysical mechanisms implied in fluorescent sensors based on such materials might also be affected by improper energy levels; i.e., high-lying HOMO levels might oxidize in biological environments.[1a] While optical properties such as absorption and emission can indicate the differences in the energy levels between the HOMO and LUMO, electrochemistry is able to further provide their exact position in the ground state. The effect of metal substitution from the d^7 Co^{II} to the d^{10} Zn^{II} in ADPM homoleptic complexes **2**−**5b** was compared to the corresponding ligands **1a** and **1b** by CV and DPV techniques (Table 1 and the Supporting Information, SI). These techniques afford critical information concerning the electronic processes occurring and exact energies associated with their HOMO/LUMO states. To complete the study, Aza-BODIPYs **6a** and **6b** are also presented.

The electrochemistry of ligands **1a** and **1b** gives an indication of the difference in stability of the ligands due to the electron-rich *p*-methoxyphenyl groups (see the SI). The irreversibility of the redox processes for **1b** may be the result of secondary reactions of the oxidized electron-rich anisole groups. This is of specific importance in the context of using derivatives based on ligand **1b** either for life science or light-harvesting system components because they are more likely to decompose over time in such environments.[1a,14a,15] While ligand **1a** presents two "pseudoreversible" oxidations of one electron each [1.01 (91) and 1.36 (137) V vs SCE] along with two other reductions [−0.78 (72) and −1.45 (16) V; Table 1], the ligand **1b** bearing four *p*-methoxyphenyl groups shows only one pseudoreversible oxidation at 0.71 (61) V followed by two irreversible peaks (1.10 and 1.30 V). The presence of a third oxidation process in ADPM ligand **1b** compared to **1a** is due to the electron-rich methoxy substituent groups. The reduction processes of **1b** are "pseudoreversible" [−0.92 (106) and −1.52 (193) V] in a fashionsimilar to the tetraphenylazadipyrromethene derivative, while being at a more negative potential.

The molecular orbitals (MOs) implied in redox processes for ADPM ligands **1a** and **1b** can be assigned by comparing the electron density map obtained from molecular modeling reported in the literature for various related ADPM and Aza-BODIPY compounds. An in silico study of interest from Russo et al. presents time-dependent density functional theory (TD-DFT) calculations for Aza-BODIPY **6a** and related −OMe derivatives in proximal and distal positions (**6c** and **6d**, respectively; Figure 4).[16] Their modelization for **6a** showed a

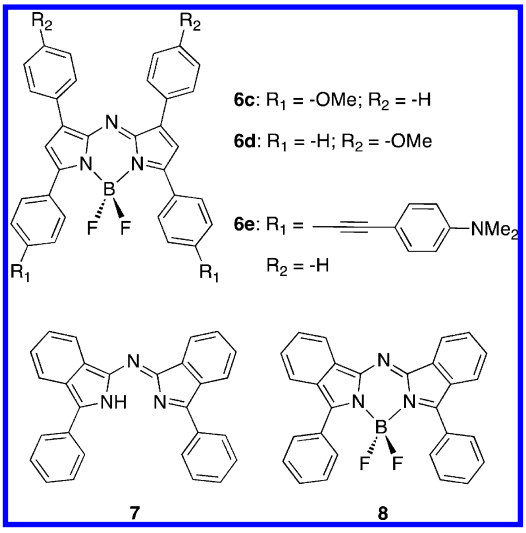

Figure 4. Related ADPM and Aza-BODIPY derivatives.

HOMO mainly based on the π system, implying the dipyrrolic core and the four phenyl rings, but with a node on the nitrogen bridge arising from C_2 symmetry in the molecule. Furthermore, the electron densities calculated for HOMO−1 and HOMO−2 were both mainly centered on the distal phenyl rings. In the case of the LUMO, delocalization throughout the whole π system was restored, including the nitrogen bridge, along with a slightly higher contribution implying the BF_2^+ fragment. On the basis of these observations, it appears reasonable to use Aza-BODIPY **6a** as a good model for the assignation of MOs from ADPM ligands **1a** and **1b**, especially because the three derivatives are symmetrical molecules. Our assignment is also supported by two other in silico studies. One was reported in

dx.doi.org/10.1021/ic300872m | Inorg. Chem. XXXX, XXX, XXX−XXX

2011 by Kobayashi et al., presenting a direct comparison between the fused-ring ADPM ligand **7** and its corresponding Aza-BODIPY derivative **8** (Figure 4). Computational studies revealed that both corresponding HOMOs and LUMOs have very similar electronic charge distribution.[6f] Jacquemin et al. lately reported analysis of the frontier orbitals of the Aza-BODIPY derivative **6e** bearing a dimethylamino electron-donating group installed in the proximal position through an extended π-conjugation system (Figure 4).[6c] Calculations for HOMO−4 to HOMO and LUMO to LUMO+4 orbitals were presented, and similarities are notable concerning the HOMO−2, HOMO−1, HOMO, and LUMO electron density localization previously reported by Russo et al. for **6a**. While the LUMO of **6e** is centered on the dipyrrolic moiety like in **6a**, the LUMO+1 to LUMO+4 of **6e** are centered on the appended phenyl rings.

Once converted into electronvolts (eV), the HOMO and LUMO levels lie at −5.95 and −4.17 eV (ΔE = 1.78 eV), respectively, for **1a**, while they are at −5.66 and −4.03 eV (ΔE = 1.63 eV) for **1b** (Table 2). A look at Scheme 2 leads to a better understanding of the electron-rich *p*-methoxyphenyl groups' effect on the energy levels of ADPM derivatives. In fact, the HOMO is easier to oxidize by about 0.29 eV in **1b** compared to **1a**. This is an indication of the additional electron density brought by the methoxy substituents. On the other hand, the first reduction of **1b** is about 0.14 eV more negative because of destabilization of the antibonding orbital. Combined, these effects decreased the energetic transition (ΔE) between the HOMO and LUMO by 0.15 eV in **1b**. In other words, the absorption band of this dye should be displaced to the red region because of a less energetic transition, as will be discussed in the absorption spectroscopy section.

Table 2. HOMO/LUMO Levels (in eV) As Determined by Electrochemistry along with ΔE Obtained from Redox and Optical Methods for ADPM Ligands 1a and 1b, Complexes 2−5b, and Aza-BODIPYs 6a and 6b

compound	chelate	HOMO[a]	LUMO[a]	ΔE_{Redox}[b]	ΔE_{Opt}[c]
1a	none	−5.95	−4.17	1.78	1.93
1b	none	−5.66	−4.03	1.63	1.81
2a	Co^{II}	−5.80	−4.02	1.78	1.69[d]
2b	Co^{II}	−5.49	−3.86	1.63	1.60[d]
3a	Ni^{II}	−5.80	−4.06	1.74	1.69[d]
3b	Ni^{II}	−5.50	−3.90	1.60	1.62[d]
4a	Cu^{II}	−5.82	−4.49	1.33	1.76[d]
4b	Cu^{II}	−5.49	−4.36	1.13	1.65[d]
5a	Zn^{II}	−5.81	−3.97	1.84	1.75[d]
5b	Zn^{II}	−5.49	−3.81	1.68	1.64[d]
6a	BF_2^+	−6.26	−4.54	1.72	1.83
6b	BF_2^+	−5.90	−4.36	1.54	1.71

[a]Reported in electronvolts. [b]Energetic difference between HOMO and LUMO obtained by electrochemistry in a DCM solution. [c]Energetic difference obtained from conversion of the emission wavelength in a DCM solution into electronvolts using the formula $E = hc/\lambda$, otherwise stated. [d]Energetic difference qualitatively obtained from the red end of the Gaussian peak of the $\lambda_{max\ shoulder}$ in a DCM solution and converted in electronvolts using the same formula as that in footnote c).

After coordination of the Lewis acidic BF_2^+ fragment, tetraphenyl-Aza-BODIPY **6a** presents a one-electron "pseudoreversible" oxidation process at 1.32 (122) V and another at 1.45 (62) V (Table 1), with the last one being limited by the potential window of DCM (see the SI). At negative potential, two "pseudoreversible" processes are present at −0.40 (101) and −1.19 (96) V. In general, the same number of redox processes is present compared to ADPM ligand **1a**, although they are all markedly stabilized by the presence of the Lewis acid chelate. For Aza-BODIPY **6b** bearing four *p*-methoxyphenyl groups, the three oxidation processes at 0.95, 1.34, and 1.52 V are irreversible. The reduction processes are, however, pseudoreversible [−0.58 (107) and −1.37 (92) V]. In a comparison of Aza-BODIPY **6b** to its ADPM ligand **1b**, the overall effect is stabilization of both the oxidation and reduction processes upon coordination of the BF_2^+ chelate.

Scheme 2. Energy Diagram (in eV) of Compounds 1−6 Including the HOMO−LUMO Difference (ΔE) As Calculated by Electrochemistry

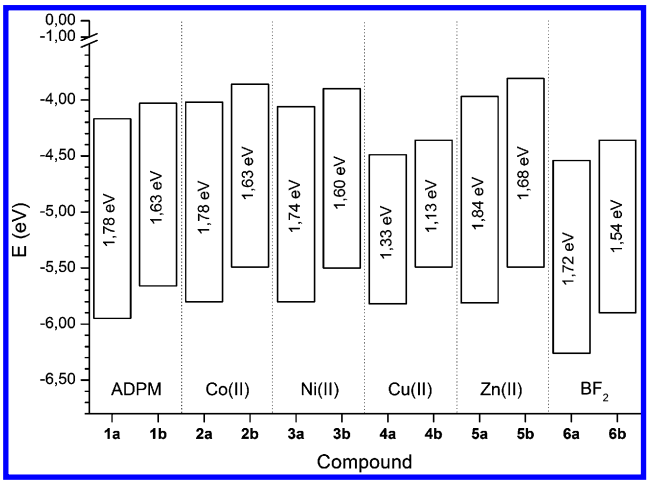

As mentioned previously in the assignation of the redox processes of ADPM ligands **1a** and **1b** from the molecular modeling of various Aza-BODIPYs,[6c,f,16] the first oxidations observed for both **6a** and **6b** are centered on the dipyrrolic core with charge stabilization throughout the appended phenyls, while the second and third (for **6b**) ones are more likely to be centered on the peripheral phenyl rings. For the reduction processes, the first reduction is based on the pyrrolic moiety, while peripheral phenyls are subsequently reduced.

A closer look at the frontier orbitals of those Aza-BODIPY derivatives shows that tetraphenyl-Aza-BODIPY **6a** presents a ligand-centered HOMO that is harder to oxidize than that of the *p*-methoxyphenyl-substituted **6b** by about 0.36 eV (−6.26 and −5.90 eV, respectively) and a ligand-centered LUMO including contributions from the BF_2^+ chelate that reduces more easily by about 0.18 eV (−4.54 and −4.36 eV, respectively; Table 2). This correlates perfectly with the observations made for **1a** and **1b** ligands arising from stabilization of the bonding orbital and destabilization of the antibonding orbital induced by the methoxy groups. In addition, the presence of the BF_2^+ electropositive fragment leads to an overall stabilization of both the HOMO and LUMO because of the Lewis base−acid interaction provided upon coordination of the chelate. For the HOMO, this stabilization is about 0.25 eV (−6.26 vs −5.95 eV for **6a** vs **1a**; −5.90 vs −5.66 eV for **6b** vs **1b**), while it is of about 0.35 eV for the LUMO (−4.54 vs −4.17 eV for **6a** vs **1a**; −4.36 vs −4.03 eV for **6b** vs **1b**). As mentioned previously, this implies a contribution from the BF_2^+ chelating agent in the first unoccupied MO of the Aza-

dx.doi.org/10.1021/ic300872m | Inorg. Chem. XXXX, XXX, XXX−XXX

BODIPYs. The computational study from Jacquemin et al. on Aza-BODIPY derivatives tends to support this hypothesis because they reported a contraction of the B−N bonds and a strong elongation of the central C−N bonds of the central rings in the S_1 excited state compared to his ground state S_0.[6c] Overall, ΔE from redox measurements decreased to 1.72 eV for **6a** and 1.54 eV for **6b**, with a relative order that correlates with the observed emission values (Tables 2 and 3).

Table 3. Compiled UV−Vis Absorption and Emission Data for Ligand 1, Complexes 2−5, and Corresponding Aza-BODIPYs 6 in DCM and THF Deaerated Solutions

		absorption[a,b]			emission[a−c]
compound	chelate	$\lambda_{max\ near\text{-}UV}$, nm ($\varepsilon$, $\times 10^3$ M^{-1} cm^{-1})	$\lambda_{max\ red}$, nm (ε, $\times 10^3$ $M^{-1}cm^{-1}$)	$\lambda_{shoulder}$, nm (ε, $\times 10^3$ $M^{-1}cm^{-1}$)	λ_{em}, nm
1a	none	302 (41)	596 (46)		644
	[d]	302 (42)	597 (47)		642
1b	none	322 (40)	627 (52)		684
	[d]	322 (41)	627 (54)		678
2a	Co^{II}	305 (64)	603 (68)	675 (41)	
	[d]	305 (64)	603 (68)	675 (40)	
2b	Co^{II}	325 (66)	632 (77)	691 (54)	
	[d]	325 (63)	632 (73)	695 (51)	
3a	Ni^{II}	306 (62)	607 (58)	653 (49)	
	[d]	306 (60)	607 (56)	655 (47)	
3b	Ni^{II}	325 (63)	631 (67)	692 (50)	
	[d]	325 (54)	631 (58)	693 (57)	
4a	Cu^{II}	303 (57)	565 (55)	640 (51)	
	[d]	303 (59)	566 (57)	641 (51)	
4b	Cu^{II}	322 (59)	591 (64)	670 (55)	
	[d]	323 (63)	591 (71)	671 (58)	
5a	Zn^{II}	304 (66)	590 (88)	644 (56)	
	[d]	303 (65)	591 (86)	642 (56)	
5b	Zn^{II}	326 (63)	612 (88)	675 (58)	
	[d]	326 (64)	613 (90)	674 (59)	
6a	BF_2^+	310 (25)	648 (80)		677
	[d]	310 (26)	651 (84)		678
6b	BF_2^+	335 (19)	691 (79)		723
	[d]	335 (19)	694 (81)		721

[a]In CH_2Cl_2 unless otherwise stated. [b]Acquisition at 293 K. [c]Value obtained from excitation at $\lambda_{max\ red}$ = 10 nm. [d]In THF (for the entire line).

When the redox behavior of homoleptic complexes **2−5b** is considered, it appears to change significantly compared to ADPM ligands **1a** and **1b** and their corresponding boron adducts **6a** and **6b**. The four main observations for the organometallic complexes (Table 2 and Scheme 2) are as follows: (i) access to one additional oxidation and one reduction process for complexes **2b−5b**; (ii) the presence of two additional reduction processes upon coordination to copper(II) for both **4a** and **4b** complexes; (iii) a general destabilization of HOMOs to the same extent throughout the metal(II) series; (iv) general stabilization of LUMOs to various extents, except for copper(II) derivatives **4a** and **4b**.

Looking at the effect of variation of the metal center on the oxidation potentials, only a slight difference is observed among the complexes for the two first oxidation potentials. Referring to the HOMO level, complexes based on **1a** are all lying between −5.80 and −5.82 eV (0.85−0.87 V), while the ones based on **1b** are between −5.49 and −5.50 eV (0.55−0.56 V). Having a HOMO energy level difference ranging from 0.30 eV for cobalt(II) complexes **2a** and **2b** to 0.33 eV for copper(II) complexes **4a** and **4b**, they all respect the relative difference of ADPM ligand **1a** compared to **1b** along with a very similar difference (0.29 eV for the ligands). These observations point toward a ligand-based HOMO, notwithstanding the slight destabilization (about 0.15 eV) by the presence of two ADPM ligands on the same homoleptic complex. This assignment of the HOMO is also in accordance with the computational models of the zinc(II) complex **5a** reported by Gray et al.[7] The second oxidation process follows the exact same behavior, with potentials ranging from 1.15 to 1.18 V for complexes based on ADPM ligand **1a** and between 0.80 and 0.82 V for the ones based on ADPM ligand **1b**. Therefore, this second pseudoreversible oxidation also seems to be ligand-based. For complexes **2b−5b**, the third irreversible oxidation process ranging between 1.19 and 1.21 V and the fourth one (also irreversible) ranging between 1.25 and 1.28 V are also pointing toward ligand-based processes because they are very similar along the metal(II) series.

While oxidation processes were slightly affected by variation of the metal center throughout the series, the trend is somewhat different for the LUMO (Scheme 2) and other reduction processes (Table 2). The presence of cobalt(II) induced stabilization of the first pseudoreversible reduction process, representing the LUMO, of 0.15 eV for complex **2a** (−4.02 eV/−0.93 V) and 0.17 eV for complex **2b** (−3.86 eV/−1.09 V) compared to their respective ADPM ligands **1a** (−4.17 eV/−0.78) and **1b** (−4.03 eV/−0.92 V). For nickel(II)-based complexes, this stabilization decreased to 0.11 and 0.13 eV for **3a** (−4.06 eV/−0.89 V) and **3b** (−3.90 eV/−1.05 V), respectively. On their side, zinc(II) complexes are showing 0.20 and 0.22 eV of LUMO stabilization for **5a** (−3.97 eV/−0.97 V) and **5b** (−3.81 eV/−1.13 V), respectively. However, all complexes based on cobalt(II), nickel(II), and zinc(II) presented a second pseudoreversible reduction process less stable than the one of their corresponding ADPM ligand by about 0.35 V for **1a** derivatives and 0.25 V for the ones based on **1b**. All three complexes based on this last ligand present an additional irreversible oxidation between −1.77 V for the zinc(II) complex **5b** and −1.80 V for the nickel(II) complex **3b**. On the basis of models of complex **5a** by Gray et al. mentioned previously,[7] all reduction processes seem to be based on the core of the ADPM ligand without significant contribution from the metal(II) present. However, variation of the metal(II) center seems to have an influence on the exact energy of the LUMO, without a clear trend going from the d^7 Co^{II} to the d^{10} Zn^{II}. Finally, the combined effect of a relatively constant HOMO with a fluctuating LUMO leads to ΔE_{Redox} = 1.78 eV for the cobalt(II) complex **2a** compared to ΔE_{Redox} = 1.63 eV for **2b**. The ΔE_{Redox} values observed are exactly the same as those found for their respective ADPM derivatives. For nickel(II) complexes, slightly smaller ΔE_{Redox} values are obtained (1.74 and 1.60 eV respectively for **3a** and **3b**), while larger ones are obtained for zinc(II) complexes (1.84 and 1.68 eV respectively for **5a** and **5b**). Overall, the ΔE_{Redox} values observed are following the same relative order as the ΔE_{Opt} ones obtained from absorption spectroscopy (Table 3).

The case of copper(II) complexes **4a** and **4b** is special because the first reduction process leads to strong destabilization (0.32 and 0.33 eV, respectively) compared to their corresponding ADPM ligands. The LUMOs are therefore low-lying at −4.49 eV (−0.46 V) and −4.36 eV (−0.59 V) for **4a**

dx.doi.org/10.1021/ic300872m | Inorg. Chem. XXXX, XXX, XXX−XXX

and **4b**, respectively. De facto, the transitions between the HOMO and LUMO levels of the two complexes are the lowest observed with ΔE_{Redox} = 1.33 eV for **4a** and ΔE_{Redox} = 1.13 eV for **4b**. Such low-lying LUMOs are attributable to the Cu^{II}/Cu^{I} reduction process in a fashion similar to that of metalloporphyrin and copper(I) phenanthroline $[Cu(NN)_2]^+$ derivatives.[17] In addition, this metal-based reduction leads to the loss of one ADPM ligand from the formally anionic complex. This explains the small pseudoreversible reduction peak observed for complexes **4a** and **4b** in CV and DPV (see the SI) around the same potentials as their corresponding ADPM ligand, i.e., at −0.80 and −0.95 V, respectively. Two other pseudoreversible processes of one electron each were observed at −1.41 (112) and −1.60 (133) V for **4a**. In the case of **4b**, these two reduction processes were irreversible (−1.54 and 1.74 V). On the basis of the related cobalt(II), nickel(II), and zinc(II) complexes, these last two reductions are attributed to the ligand.

Optical Properties. To complete our study of ADPM dye derivatives in coordination chemistry, absorption and emission spectra of the newly synthetized complexes **2b**−**5b** and Aza-BODIPY **6b** based on ligand **1b** were recorded (Figures 5 and

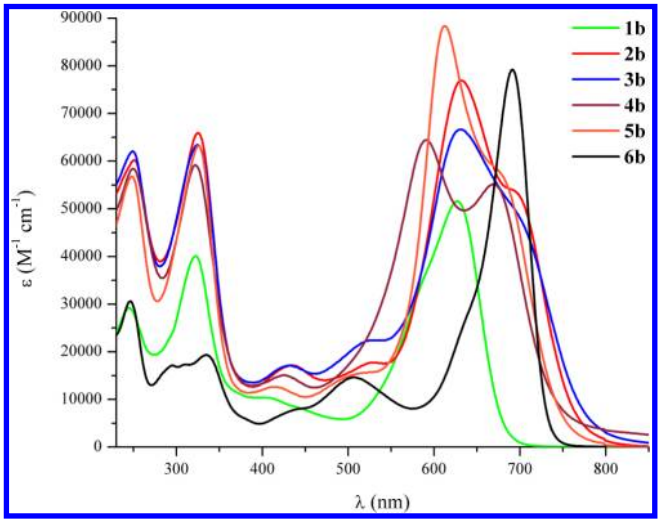

Figure 5. Absorption spectra of ligand **1b**, complexes **2b**−**5b**, and Aza-BODIPY **6b** in DCM.

6, respectively). In a desire to standardize and complete the various data available in the existing literature, data were collected for ligand **1a**, complexes **2a**−**5a**, and Aza-BODIPY **6a** in both DCM and THF (Table 3). All together, this information should lead to a better understanding of trends arising from variation of the electronic density of the ligand and/or coordinated center.

The presence of four electron-rich methoxy groups on **1b** led to a bathochromic shift of 37 nm in DCM and 31 nm in THF compared to **1a**. In fact, λ_{max} in the red region for **1b** was of 627 nm in both solvents, compared to 590 nm in DCM and 596 nm in THF for **1a**. Such a bathochromic shift follows the tendency observed in the literature as the presence of two *p*-methoxy substituents in the distal position gave a λ_{max} at 607 nm and at 620 nm in the proximal position (in THF).[7] A further comparison can be made between ADPM ligand **1a** and its tetraphenyldipyrromethene derivative reported by Guy and Jones.[18] In this case, a bathochromic shift of 50 nm is observed simply based on the presence of the nitrogen atom on the

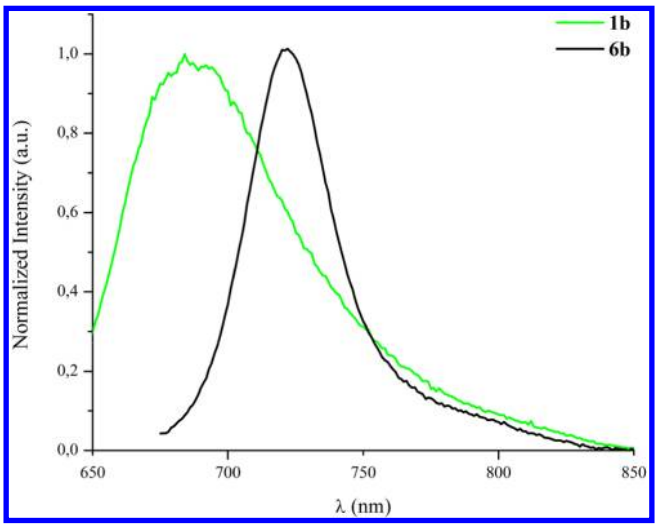

Figure 6. Emission spectra of **1b** and **6b** in DCM.

bridge of the ADPM. Typical of ADPM dyes, a second absorption band is observed in the 300 nm region ($\lambda_{max\ near\text{-}UV}$) arising from variable orbital contributions, mainly $\pi-\pi^*$ transitions, depending of the substituents present in the chromophore.[6c] As mentioned by Jacquemin and co-workers, these orbital contributions are hard to formally establish without in silico simulations.[6c,19] Also of interest, **1b** offers a molar absorptivity (ε) of 54000 M^{-1} cm^{-1} in THF, about 20% more than any of the other *p*-methoxy-substituted or tetraphenyldipyrromethenes. They are also on the same order of magnitude as what was observed by Gresser and co-workers for benzannulated ADPM derivatives that exhibit better π conjugation.[6g] In fluorescence spectroscopy, **1a** presents an emission at 644 nm in DCM, which shifts negligibly in more polar THF (642 nm). ADPM ligand **1b** exhibited an emission centered at 684 nm in DCM (Figure 6), with a larger hypsochromic effect of 6 nm compared to **1a**, bringing the emission up to 678 nm in THF (see the SI). Emission peaks are tailing out to approximately 850 nm in both solvents, which make ADPM ligand **1b** an interesting candidate for NIR applications. Once converted into electronvolts, the optical band gap (ΔE_{Opt}) can be compared to the one obtained by electrochemistry (ΔE_{Redox}) in order to evaluate whether the trends are respected. While the values of the band gap do not correspond perfectly between redox and optical measurements (1.78 vs 1.93 eV, respectively, for **1a** and 1.63 vs 1.81 eV for **1b**), the relative order within each method is respected (Table 2).

The presence of two ligands brought into proximity by a metallic center in homoleptic complexes **2**−**5** gives rise to interesting behavior. As explained by O'Shea et al. for the copper(II) complex **4a**, the clear splitting of the longest wavelength band with λ values of 565 and 640 nm in DCM (slight bathochromic shift of 1 nm in THF for both λ values) is indicative of the strain within the ligand.[8] The same behavior is observed for the copper(II) complex **4b** bearing the four *p*-methoxy groups, with λ values red-shifted to 591 and 670 nm in DCM (slight bathochromic shift of 1 nm in THF for the second λ value only). For complexes **2**, **3**, **5a**, and **5b**, only a distinct red-shifted shoulder ($\lambda_{shoulder}$) of the main absorption band $\lambda_{max\ red}$ is observed. In that last series of complexes, only a slight shift is discernible between the $\lambda_{shoulder}$ recorded in DCM and THF, in the margin of error of the measurements.

dx.doi.org/10.1021/ic300872m | Inorg. Chem. XXXX, XXX, XXX−XXX

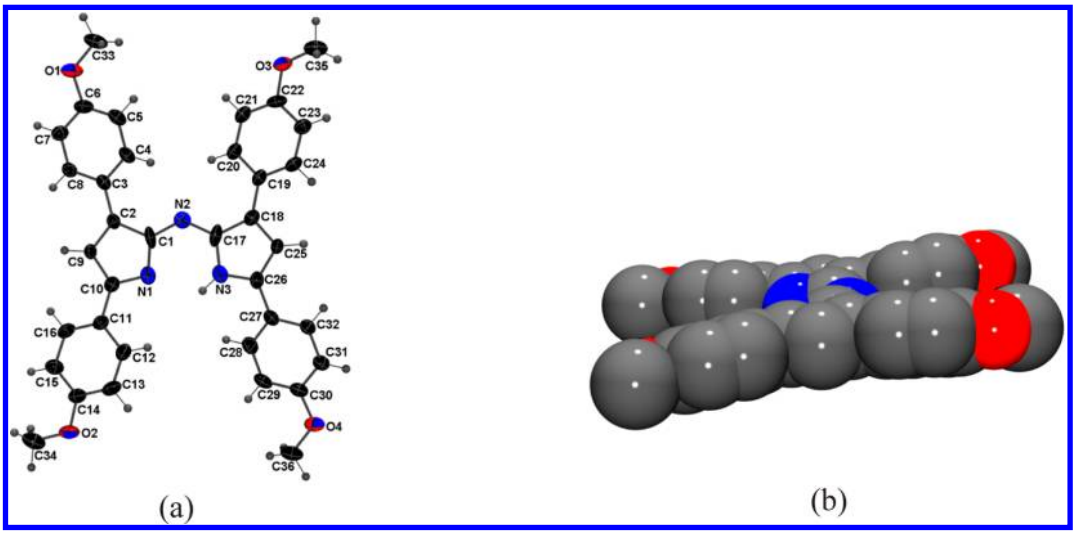

Figure 7. (a) Thermal ellipsoid projection of the ligand **1b** (ellipsoids are shown at 30% probability). (b) Space-filling model of the view of L along the central plane, showing the tilt of the rings. The hydrogen atoms were omitted for clarity. Selected bond lengths (Å) and angles (deg): N1−C1 1.407(5), N1−C10 1.348(4), N2−C1 1.327(4), N2−C17 1.319(4), N3−C17 1.374(5), N3−C26 1.361(4); C1−N2−C17 126.5(3), N1−C1−N2 121.2(3), N2−C17−N3 122.3(3).

Complexes **2b**−**5b** presented a bathochromic shift in DCM of $\lambda_{\text{max red}}$ compared to their tetraphenyl counterpart ranging from 22 nm between zinc(II) complexes to 29 nm between cobalt(II) ones. As mentioned previously, the molar absorptivity of ligand **1b** was higher than that for **1a**, and this trend transferred to the homoleptic complexes. Through the series, metal(II) complexes based on ligand **1b** exhibit a higher molar absorptivity by roughly 9000 M^{-1} cm^{-1} compared to the ones based on ADPM ligand **1a** in a DCM solution, except for zinc(II) complexes, where no difference is observed. The more polar THF solution seems to yield the same overall trend but with lower values, in general, than those in a DCM solution. Both copper(II) complexes present an absorption spectrum in the red region similar to their respective ligand and related metal(II) complexes, which means that electronic transitions observed in that absorption region possess mainly a cyanine-like character, which implies $\pi-\pi^*$ transitions.[6c] This observation further supports the idea that the first reduction process observed by electrochemistry is metal-centered on the Cu^{II}/Cu^{I} process. Similar to what was reported by Gray and O'Shea about homoleptic metal(II) complexes bearing ADPM derivatives, no emission was observed for the newly synthesized complexes **2b**−**5b**. Therefore, a comparison of the band-gap values with redox measurements needs to be done based on an optical band gap evaluated using the intersection of the end of $\lambda_{\text{shoulder}}$ with the baseline (edge absorption; Table 2). Again, a direct comparison of values obtained by redox versus optical measurements for a given compound shows that they do not match perfectly. A systematic underestimation from the latter method is observed, still giving values that are closer compared to those obtained from the emissive compounds. However, the relative order between given metal(II) complexes based on ADPM ligand **1a** vs **1b** is consistent.

Aza-BODIPYs **6a** and **6b** absorb in the red region ($\lambda_{\text{max red}}$) at 648 and 691 nm, respectively, in a DCM solution. Measurements in a THF solution give rise to a red shift of 3 nm in both cases. The bathochromic shift induced by the presence of the tetrakis(*p*-methoxyphenyl) substituents reached 43 nm, slightly more than that for the parent ADPM ligands. The molar absorptivities of **6a** (84000 M^{-1} cm^{-1} in THF) and **6b** (81000 M^{-1} cm^{-1}) are significantly increased compared to their ADPM precursors **1a** and **1b**, a typical behavior in this family of chromophore.[20] In addition, the presence of four electron-rich −OMe groups in **6b** gave a 46 cm^{-1} bathochromic shift in DCM to the sharp emission at 723 nm compared to tetraphenyl **6a** (677 nm). Similar emission values were observed in THF and are consistent with the shift observed in absorption and the tailing of the emission band out to 850 nm, in a fashion similar to that of ADPM ligand **1b**, which shows potential for NIR applications if photo- and chemo-stability can be ensured in the given system. Concerning the band gaps, ΔE_{Opt} is systematically overestimated, as was found for ADPM ligands **1a** and **1b**; however, the relative order obtained is consistent for the two methods.

X-ray Diffraction. The slow diffusion of hexanes into a CH_2Cl_2 solution at rt of **1b** and **2b** afforded single crystals for X-ray crystallography. Both compounds crystallized in the monoclinic space group $P2_1/c$ (see the SI). The molecular structure of the ligand **1b** confirms the conjugated nature of the azadipyrrole unit, with bond lengths for the bridging nitrogen to both pyrrole rings of 1.330(4) and 1.319(4) Å for N2−C1 and N2−C17, respectively (Figure 7a). All other bond distances are in the expected range for those found in conjugated systems of this type of chromophore. As previously observed for other ADPM derivatives,[8] these structures show two very planar central pyrrolic rings [the angle of intersection between the two is negligible at 1.29(3)°] and four twisted *p*-methoxyphenyl groups. Of interest, ADPM ligand **1b** features internal asymmetry relative to the pyrrolic rings in the solid state, which is due to tautomerism for the pyrrole hydrogen. The structure was therefore refined with a disordered hydrogen atom on N1 and N3 atoms, leading to a ratio of about 1:2 in favor of N3. In addition, the distance between the centroids of the phenyl rings in position 3 of the pyrrolic ring is slightly shorter compared to the ones in position 5 [6.29(5) and 7.12(5) Å, respectively]. Also, the tilt between the rings formed by the azadipyrrole moiety and the phenyl rings varies from 24.62(9)° for distal positions to only 18.47(8)° for proximal ones.

dx.doi.org/10.1021/ic300872m | *Inorg. Chem.* XXXX, XXX, XXX−XXX

The crystal structure of the homoleptic cobalt(II) complex **2b** is shown in Figure 8. The two ADPM bidentate ligands **1b**

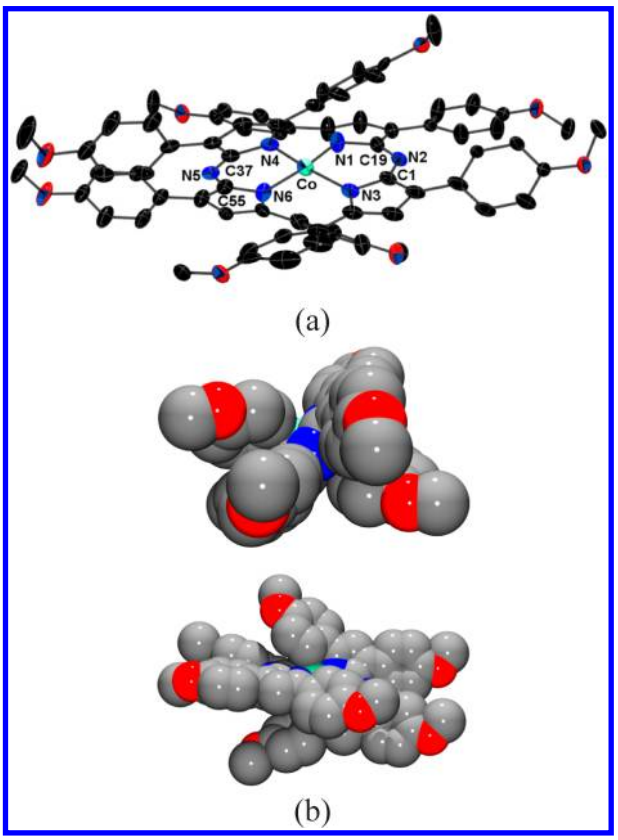

Figure 8. Thermal ellipsoid projection of cobalt(II) complex **2b** (the disorder over the methoxyphenyl rings, corresponding to 30% of the occupancy factor, was omitted for clarity). (a) Ellipsoids are shown at 30% probability (the labeling and hydrogen atoms were omitted for clarity). Selected bond lengths (Å) and angles (deg): Co−N1 1.975(3), Co−N3 1.987(3), Co−N4 1.992(3), Co−N6 1.975(2); N1−Co−N4 106.55(12), N3−Co−N6 108.08(11), N1−Co−N6 128.68(11), N3 −Co-N4 128.22(11). (b) Space-filling model of the view of Co along the N2−Co−N5 plane and N1−Co−N6, showing the tilt of the rings. The hydrogen and disordered atoms were omitted for clarity.

force a distorted tetrahedral geometry at the metal center, with Co−N bond distances ranging from 1.975(2) Å for Co−N6 to 1.992(3) Å for Co−N4 and chelate angles of N1−Co−N3 [94.7(1)°] and N4−Co−N6 [94.5(1)°] being slightly different from each other. Other bond distances and angles are generally very similar to those found by Gray and O'Shea for related complexes.[7,8] As expected, the chelating ligand is planar, with an angle between best-fit planes of 67°. The crystal structure of **2b** also revealed that, upon coordination of the ligands, the phenyl rings arrange in a clockwise fashion (Figure 8b), although no significant π interaction was found in the crystal packing. Again, this behavior compares with similar complexes reported by Gray and O'Shea.

CONCLUSIONS

In summary, we reported herein a high-yielding microwave-assisted synthesis of four new homoleptic complexes of cobalt(II), nickel(II), copper(II), and zinc(II) based on **1b**. These complexes were compared with already known ADPM homoleptic complexes of the same metal(II) series and related BF_2^+ chelates (Aza-BODIPY) for a better understanding of trends arising from substitution of the chelate and/or electron-donating effect of the *p*-methoxy substituents. Electrochemical characterization revealed four main observations for the organometallic complexes: (i) access to one additional oxidation and one reduction process for complexes **2b**−**5b** compared to related ADPM ligand **1b**; (ii) the presence of two additional reduction processes upon coordination to copper(II) for both **4a** and **4b** complexes; (iii) a general destabilization of HOMOs to the same extent throughout the metal(II) series; (iv) a general stabilization of LUMOs to various extents, except for copper(II) derivatives **4a** and **4b**. These two copper(II) complexes presented a metal-centered first reduction process (Cu^{II} to Cu^{I}) that engenders decoordination of one ADPM ligand and also a lower ΔE_{Redox} compared to related complexes. Optical characterization further supports this hypothesis by exhibiting similar absorption properties for copper(II) complexes compared to cobalt(II), nickel(II), and zinc(II) ones and their free ligands. Such behavior is indicative of a cyanine-like character, implying mainly $\pi-\pi^*$ transitions. As might be expected from electron-rich −OMe substituents, emission of**1b** and Aza-BODIPY derivative **6b** gave a bathochromic shift compared to related tetraarylazadipyrromethene compounds previously reported. X-ray structures for **1b** and related cobalt(II) complex **2b** were also presented.

ASSOCIATED CONTENT

Supporting Information

HR-ESIMS for newly synthesized complexes **2b**−**5b**, cyclic and differential pulse voltammograms for ADPM **1a** and **1b**, complexes **2**−**5b**, and Aza-BODIPYs **6a** and **6b**, absorption spectra in DCM for ADPM **1a**, complexes **2a**−**5a**, and Aza-BODIPY **6a**, absorption spectra in THF for ADPM **1a** and **1b**, complexes **2**−**5b**, and Aza-BODIPYs **6a** and **6b**, emission spectra in DCM for **1a** and **6a**, emission spectra in THF for **1a**, **1b**, **6a**, and **6b**, crystal data and details of the structure determination for **1b** (CCDC 876955) and **2b** (CCDC 876954) along with the ORTEP representation of **2b** at the 50% probability level, and X-ray crystallographic data in CIF format. This material is available free of charge via the Internet at http://pubs.acs.org.

AUTHOR INFORMATION

Corresponding Author

*E-mail: garry.hanan@umontreal.ca. Tel: +1 514 340 5156. Fax: +1 514 343 7586.

Notes

The authors declare no competing financial interest.

ACKNOWLEDGMENTS

G.S.H. thanks the Natural Sciences and Engineering Research Council of Canada, the Centre for Self-Assembled Chemical Structures, and the Université de Montréal (UdeM) for financial support. A.B. thanks NSERC, FQRNT, and Saint-Jean Photochemicals Inc. (sjpc.com) for a BMP-Innovation grant. J.G.F. is thankful to the Canadian Postdoctoral Research Fellowship Programme. The authors also thank Anne-Catherine Bédard, Daniel Chartrand, and the Combinational Chemistry, NMR, Mass Spectrometry, Elemental Analysis, and X-ray laboratories of UdeM for their help.

REFERENCES

(1) (a) Boens, N.; Leen, V.; Dehaen, W. *Chem. Soc. Rev.* **2012**, *41*, 1130−1172. (b) Ulrich, G.; Ziessel, R.; Harriman, A. *Angew. Chem., Int. Ed.* **2008**, *47*, 1184−1201. (c) Smith, N. W.; Alonso, A.; Brown, C. M.; Dzyuba, S. V. *Biochem. Biophys. Res. Commun.* **2010**, *391*, 1455−1458. (d) Nierth, A.; Kobitski, A. Y.; Nienhaus, G. U.; Jaschke, A. *J. Am. Chem. Soc.* **2010**, *132*, 2646−2654. (e) Buyukcakir, O.; Bozdemir, O. A.; Kolemen, S.; Erbas, S.; Akkaya, E. U. *Org. Lett.* **2009**, *11*, 4644−4647. (f) Nepomnyashchii, A. B.; Bard, A. J. *Acc. Chem. Res.* **2012**, DOI: 10.1021/ar200278b.

(2) (a) Ziessel, R.; Harriman, A. *Chem. Commun.* **2011**, *47*, 611−631. (b) Iehl, J.; Nierengarten, J.-F.; Harriman, A.; Bura, T.; Ziessel, R. *J. Am. Chem. Soc.* **2012**, *134*, 988−998. (c) Kolemen, S.; Bozdemir, O. A.; Cakmak, Y.; Barin, G.; Erten-Ela, S.; Marszalek, M.; Yum, J.-H.; Zakeeruddin, S. M.; Nazeeruddin, M. K.; Gratzel, M.; Akkaya, E. U. *Chem. Sci.* **2011**, *2*, 949−954. (d) Bozdemir, O. A.; Yilmaz, M. D.; Buyukcakir, O.; Siemiarczuk, A.; Tutas, M.; Akkaya, E. U. *New J. Chem.* **2010**, *34*, 151−155. (e) Rio, Y.; Seitz, W.; Gouloumis, A.; Vazquez, P.; Sessler, J. L.; Guldi, D. M.; Torres, T. *Chem.—Eur. J.* **2010**, *16*, 1929−1940.

(3) (a) Teets, T. S.; Partyka, D. V.; Esswein, A. J.; Updegraff, J. B., III; Zeller, M.; Hunter, A. D.; Gray, T. G. *Inorg. Chem.* **2007**, *46*, 6218−6220. (b) Partyka, D. V.; Deligonul, N.; Washington, M. P.; Gray, T. G. *Organometallics* **2009**, *28*, 5837−5840. (c) Teets, T. S.; Updegraff, J. B., III; Esswein, A. J.; Gray, T. G. *Inorg. Chem.* **2009**, *48*, 8134−8144.

(4) Loudet, A.; Burgess, K. *Chem. Rev.* **2007**, *107*, 4891−4932.

(5) (a) Hall, M. J.; McDonnell, S. O.; Killoran, J.; O'Shea, D. F. *J. Org. Chem.* **2005**, *70*, 5571−5578. (b) Yakubovskyi, V. P.; Shandura, M. P.; Kovtun, Y. P. *Synth. Commun.* **2010**, *40*, 944−950. (c) Li, Y.; Dolphin, D.; Patrick, B. O. *Tetrahedron Lett.* **2010**, *51*, 811−814.

(6) (a) Bellier, Q.; Dalier, F.; Jeanneau, E.; Maury, O.; Andraud, C. *New J. Chem.* **2012**, *36*, 768−773. (b) Amin, A. N.; El-Khouly, M. E.; Subbaiyan, N. K.; Zandler, M. E.; Fukuzumi, S.; D'Souza, F. *Chem. Commun.* **2012**, *48*, 206−208. (c) Le Guennic, B.; Maury, O.; Jacquemin, D. *Phys. Chem. Chem. Phys.* **2012**, *14*, 157−164. (d) D'Souza, F.; Amin, A. N.; El-Khouly, M. E.; Subbaiyan, N. K.; Zandler, M. E.; Fukuzumi, S. *J. Am. Chem. Soc.* **2011**, *134*, 654−664. (e) Batat, P.; Cantuel, M.; Jonusauskas, G.; Scarpantonio, L.; Palma, A.; O'Shea, D. F.; McClenaghan, N. D. *J. Phys. Chem. A* **2011**, *115*, 14034−14039. (f) Lu, H.; Shimizu, S.; Mack, J.; Shen, Z.; Kobayashi, N. *Chem.—Asian J.* **2011**, *6*, 1026−1037. (g) Gresser, R.; Hummert, M.; Hartmann, H.; Leo, K.; Riede, M. *Chem.—Eur. J.* **2011**, *17*, 2939−2947. (h) Gao, L.; Senevirathna, W.; Sauvé, G. v. *Org. Lett.* **2011**, *13*, 5354−5357. (i) Tasior, M.; Murtagh, J.; Frimannsson, D. O.; McDonnell, S. O.; O'Shea, D. F. *Org. Biomol. Chem.* **2010**, *8*, 522−525. (j) Yuan, M.; Yin, X.; Zheng, H.; Ouyang, C.; Zuo, Z.; Liu, H.; Li, Y. *Chem.—Asian J.* **2009**, *4*, 707−713. (k) Mueller, T.; Gresser, R.; Leo, K.; Riede, M. *Sol. Energy Mater. Sol. Cells* **2012**, *99*, 176−181. (l) Leblebici, S. Y.; Catane, L.; Barclay, D. E.; Olson, T.; Chen, T. L.; Ma, B. *ACS Appl. Mater. Interfaces* **2011**, *3*, 4469−4474.

(7) Teets, T. S.; Partyka, D. V.; Updegraff, J. B.; Gray, T. G. *Inorg. Chem.* **2008**, *47*, 2338−2346.

(8) Palma, A.; Gallagher, J. F.; Mueller-Bunz, H.; Wolowska, J.; McInnes, E. J. L.; O'Shea, D. F. *Dalton Trans.* **2009**, 273−279.

(9) Rogers, M. A. T. *J. Chem. Soc.* **1943**, 590−596.

(10) (a) Rousseau, T.; Cravino, A.; Ripaud, E.; Leriche, P.; Rihn, S.; De Nicola, A.; Ziessel, R.; Roncali, J. *Chem. Commun.* **2010**, *46*, 5082−5084. (b) Kubo, Y.; Watanabe, K.; Nishiyabu, R.; Hata, R.; Murakami, A.; Shoda, T.; Ota, H. *Org. Lett.* **2011**, *13*, 4574−4577.

(11) *APEX2*; Bruker AXS Inc.: Madison, WI, 2009.

(12) Sheldrick, G. M. *SADABS*, Bruker AXS Inc.: Madison, WI, 1996.

(13) *SHELXTL*, version 6.12; Bruker AXS Inc.: Madison, WI, 2001.

(14) (a) Mishra, A.; Bäuerle, P. *Angew. Chem., Int. Ed.* **2012**, *51*, 2020−2067. (b) Li, Y. *Acc. Chem. Res.* **2012**, *45*, 723−733.

(15) (a) Blouin, N.; Michaud, A.; Gendron, D.; Wakim, S.; Blair, E.; Neagu-Plesu, R.; Belletête, M.; Durocher, G.; Tao, Y.; Leclerc, M. *J. Am. Chem. Soc.* **2007**, *130*, 732−742. (b) Zeng, L.; Jiao, C.; Huang, X.; Huang, K.-W.; Chin, W.-S.; Wu, J. *Org. Lett.* **2011**, *13*, 6026−6029. (c) Jørgensen, M.; Norrman, K.; Gevorgyan, S. A.; Tromholt, T.; Andreasen, B.; Krebs, F. C. *Adv. Mater.* **2012**, *24*, 580−612.

(16) Quartarolo, A. D.; Russo, N.; Sicilia, E. *Chem.—Eur. J.* **2006**, *12*, 6797−6803.

(17) (a) Smith, K. M. *Porphyrins and Metalloporphyrins*; Elsevier: New York, 1975; p 910. (b) Armaroli, N. *Chem. Soc. Rev.* **2001**, *30*, 113−124. (c) Accorsi, G.; Armaroli, N.; Duhayon, C.; Saquet, A.; Delavaux-Nicot, B.; Welter, R.; Moudam, O.; Holler, M.; Nierengarten, J.-F. *Eur. J. Inorg. Chem.* **2010**, *2010*, 164−173.

(18) Guy, R.; Jones, R. *Aust. J. Chem.* **1966**, *19*, 1871−1885.

(19) (a) Jacquemin, D.; Planchat, A.; Adamo, C.; Mennucci, B. *J. Chem. Theory Comput.* **2012**, *8*, 2359−2372. (b) Chibani, S.; Le Guennic, B.; Charaf-Eddin, A.; Maury, O.; Andraud, C.; Jacquemin, D. *J. Chem. Theory Comput.* **2012**, 3303−3313.

(20) Gorman, A.; Killoran, J.; O'Shea, C.; Kenna, T.; Gallagher, W. M.; O'Shea, D. F. *J. Am. Chem. Soc.* **2004**, *126*, 10619−10631.